A facile way to optimize thermoelectric properties of SnSe thin films via sonication-assisted liquid-phase exfoliation

Thiet Van Duong[1,*] , Nguyen Xuan Chung[2], Hong Ngoc Phan[3], Hong Tuan Nguyen[3], Dung Dinh Nguyen[3], Lu Trong Le[4], and Nhat Van Pham[5]

[1] *Graduate University of Science and Technology, Vietnam Academy of Science and Technology, Hanoi 100000, Vietnam*

[2] *Department of Physics, Hanoi University of Mining and Geology, Hanoi 100000, Vietnam*

[3] *Center for High Technology Development, Vietnam Academy of Science and Technology, Hanoi 100000, Vietnam*

[4] *Institute for Tropical Technology, Vietnam Academy of Science and Technology, Hanoi 100000, Vietnam*

[5] *Department of Advanced Materials Science and Nanotechnology, University of Science and Technology Hanoi, Hanoi 100000, Vietnam*

ABSTRACT

In our work, SnSe nanosheets and nanostructured thin films were successfully synthesized via sonication-assisted exfoliation and coating process. The SnSe nanosheets respond to a uniform lateral size, with two to three single layers by 2.82 nm and 280 nm^2 of average thickness and average area, respectively. The results were confirmed by Scanning Electron Microscope, Transmission Electron Microscope, and Atomic Force Microscope. X-ray diffraction and Raman spectra indicate that the SnSe nanosheets have high crystalline quality along *a*-axis. The SnSe nanostructured thin films were prepared in various thicknesses from 350 to 650 nm. The highest power factor value is achieved at 450 nm in 375–600 K temperature range. A simple method of fabrication and controllable thermoelectric properties of SnSe nanostructured thin films as well as other two-dimensional (2D) materials are introduced.

1 Introduction

Recently, the researches on high-performance thermoelectric materials have been withdrawn great attention in both industry and academic because of their promising potentials in harvesting waste-heat energy from industrial factories [1–4], thermoelectric generator, and all-solid-device in vehicles [5, 6]. The device performance strongly depends on the properties of thermoelectric materials which is manifested through the Figure of merit ZT = $(S^2\sigma T)/\kappa$, where σ is the electrical conductivity, S is Seebeck coefficient, T is absolute temperature, and κ is thermal conductivity. Fundamentally, the thermoelectric materials with a high-power factor (PF = $S^2\sigma$) and a low thermal conductivity (κ) can achieve a high ZT value.

Among the efficient materials, Bi_2Te_3 and PbTe are the state-of-art materials owing to their low thermal conductivity and high metallic states [7–9]. However, the applications of these materials and their alloys are still limited due to the presence of harmful heavy metals, expensive raw materials, and complicated manufacturing conditions [10–14]. Recently, SnSe has been an attractive material because of its excellent intrinsic thermoelectric characteristics, low toxicity, and abundance [15–18]. At 300 K, this material possess a low thermal conductivity (0.6 W/mK) and a remarkable Seebeck coefficient (520 µV/K) which is higher than that of Bi_2Te_3 (180 µV/K) and of PbTe (370 µV/K). This outstanding performance of SnSe can originate from strong anharmonicity of Sn–Se chemical bonding and layered structure [19–21]. As reported in the literature, SnSe nanostructures enhance their thermoelectric properties than their bulk materials in which photon scattering leads to reducing thermal conductivity. However, SnSe nanostructures still need more intensive researches [22–24].

In this study, we demonstrate the synthesis of SnSe nanosheets (NSs) by sonication-assisted solution-based exfoliation method. Under sonication condition, the tetrabutylammonium bromide (TBAB) is intercalated into SnSe layers then makes them peel off the bulk material to form NSs. The as-exfoliated SnSe NSs show average size of 280 nm^2 with a narrow size distribution. Furthermore, the 2D SnSe NSs contain two to three single layers with an average thickness of 2.82 nm. The X-ray diffraction (XRD) spectroscopy, Raman, and X-ray photoelectron spectroscopy (XPS) show the high crystalline quality of SnSe NSs. The SnSe nanostructured thin films were also prepared to test thermoelectric performance by using spray coating methods. It is found that the thin films with thickness of 450 nm relate to significant enhancement of PF in temperature range of 375–600 K.

2 Experiment

2.1 Materials and reagents

All chemicals and solvents without purification were purchased from the Sigma-Aldrich, and deionized water (DI) was produced by a Milli-Q Millipore system (18.2 MΩ, Millipore Corp, Billerica, MA).

2.2 Preparation of SnSe NSs

In order to prepare 2D SnSe NSs, the molecule intercalation method and liquid-phase-exfoliation-sonication-assisted extraction were applied. An amount of 100 g of tetrabutylammonium bromide (TBAB) powder was gradually dissolved in 50 mL DI water and then became a transparent solution under magnetic stirring at room temperature. Next, 0.5 g bulk SnSe powder (99.5%) was added into the above solution and was stirred steadily. The obtained solution was transferred into a beaker followed by sonication process by a 100 W ultrasonic tip for 24 h in an ice bath to avoid oxidation of the SnSe NSs. Consequently, the formed solution was centrifuged at 5000 rpm for 30 min to remove residual bulk SnSe. Finally, dispersive SnSe was collected by filtration again, and then, SnSe was transferred into iso-propanol (IPA) solvent with a concentration of 1 mg/mL for further characterization.

2.3 Fabrication of SnSe nanostructured thin films

Some 2×2 cm^2 SiO_2 (300 nm of thickness)/Si substrates were first treated by UV Ozone to enhance hydrophilicity of the surface, then 0.4 mL of SnSe solution in IPA (1 mg/mL) was sprayed onto the preheated SiO_2/Si substrate using an airbrush system with Argon as a carrier gas. The airbrush (Richpen 112B, Japan) with a 0.2 mm-diameter nozzle was set at single action mode with the pressure of 2 bar. The distance between the substrate and the spraying gun was set at 10 cm. The substrate was heated at 60 °C during spraying process.

2.4 Characterization methods

The topographic roughness of the SnSe NSs deposited on a silica substrate was characterized using taping mode of an Atomic Force Microscopy (AFM) Veeco, Dimension 3100. The nanostructures were observed by Transmission Electron Microscope (TEM, JEOL) and High-Resolution TEM (HR-TEM, JEM-2100F). The XPS (Thermo Fisher) measurements were conducted by using monochromatic Al-Kα radiation (hv = 1486.6 eV). The Raman spectrum was measured from 50 to 2000/cm at room temperature using DXR Raman spectrometer with a 532 nm-excitation source (Thermo Scientific). A commercial

equipment Ulvac ZEM-3 (ULVAC, Methuen, MA, USA) with temperature differential mode and four-probe configuration was used for the measurements on Seebeck coefficient and electrical conductivity, respectively, inside a chamber filled with helium gas at the low pressure.

3 Results and discussion

The facile synthetic strategy to produce SnSe NSs based on exfoliation method is illustrated in Fig. 1. Under ultrasonication condition, the TBAB first was intercalated into SnSe layers along b–c plane due to its smaller molecules size than distance between two adjacent layers along axis a (1.15 nm) which is held by a weak interlayer van der Waals interaction. TBA$^+$ cations can effectively attach at the negative surface of SnSe via electrostatic interaction that enhances exfoliation efficiency. During sonication, agitations cause forceful vibration of individual SnSe layer, more TBA$^+$ molecules are inserted into the between interlayers, that leads to volume expansion inside SnSe crystal and weakens layer–layer interaction. As a result, the SnSe layers are efficiently cleaved, and exfoliated SnSe NSs are produced.

The morphology of synthesized SnSe NSs was characterized by Scanning Electron Microscope (SEM) and TEM. As shown in Fig. 2a and b, the uniform lateral size of SnSe NSs is easily seen and indicates the success of exfoliation process. Figure 2c represents HR-TEM images which clearly reveal lattice distance of 0.288 nm, assigning to the (400) face of SnSe [25]. The analysis of TEM images in Fig. 2d shows a large size distribution of synthesized SnSe sheets with an average area of 280 nm^2.

The topology and thickness profile of SnSe NSs were studied by AFM. The sample was prepared by spin coating SnSe NSs solution (0.5 mg/mL) on a silica substrate. Figure 3a shows an AFM image of SnSe NSs with the thickness around 2 nm. Most of the exfoliated SnSe NSs have similar thickness and similar area. As reported in some literatures, the thickness of a single layer SnSe sheets is 1 nm [26], hence our synthesized SnSe NSs contain two or three single layers. The thickness histogram in Fig. 3b is statistically analyzed for 450 NSs, it illustrates a narrow distribution in which there are above 50% number of sheets performing the thickness of around 2 nm, the average thickness for all NSs is 2.82 nm.

In order to determine the crystal quality of the as-prepared SnSe NSs, XRD and Raman spectroscopy were carried out. The sample was prepared by coating the exfoliated SnSe NSs solution on a SiO$_2$/Si substrate (SiO$_2$ 300 nm thickness). Figure 3c displays the XRD patterns of SnSe bulk and exfoliated SnSe NSs. The patterns reveal that the SnSe NSs belong to orthorhombic SnSe crystal structure (*Pmma* space group) at room temperature. It is clearly observed that (400) peak position of the SnSe NSs shows lower diffraction angle than that of bulk SnSe. This downward shift indicates the volume expansion in lattice along a-axis which demonstrates that TBA$^+$ cations successfully intercalate into crystal structure of SnSe. Importantly, the (400) peak exhibits the strongest intensity among all peaks, confirms the high
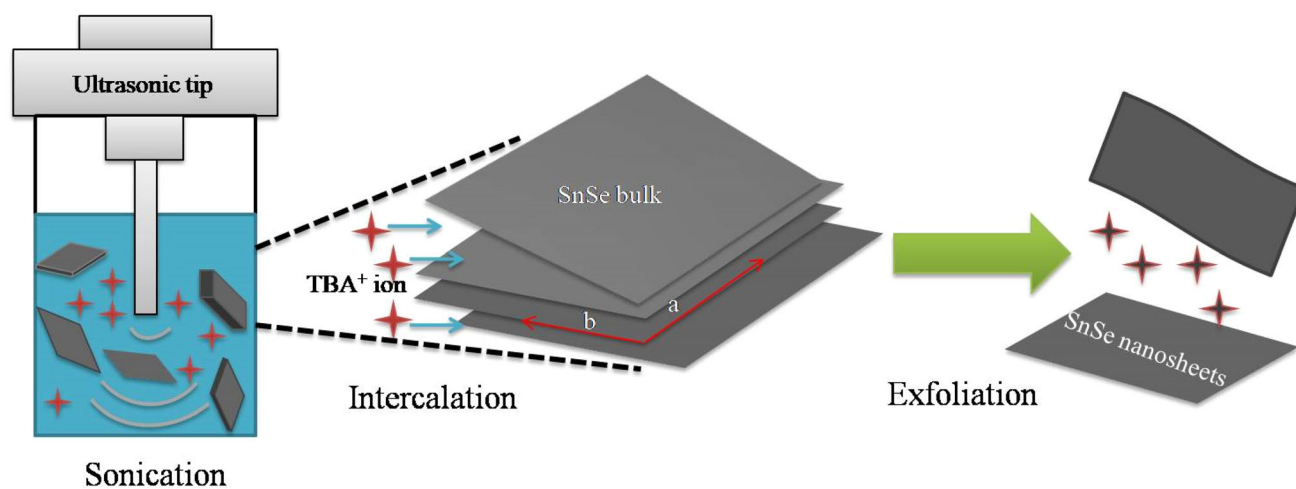

Fig. 1 Schematic illustration for TBAB (red star)-assisted liquid-phase exfoliation of SnSe (Color figure online)
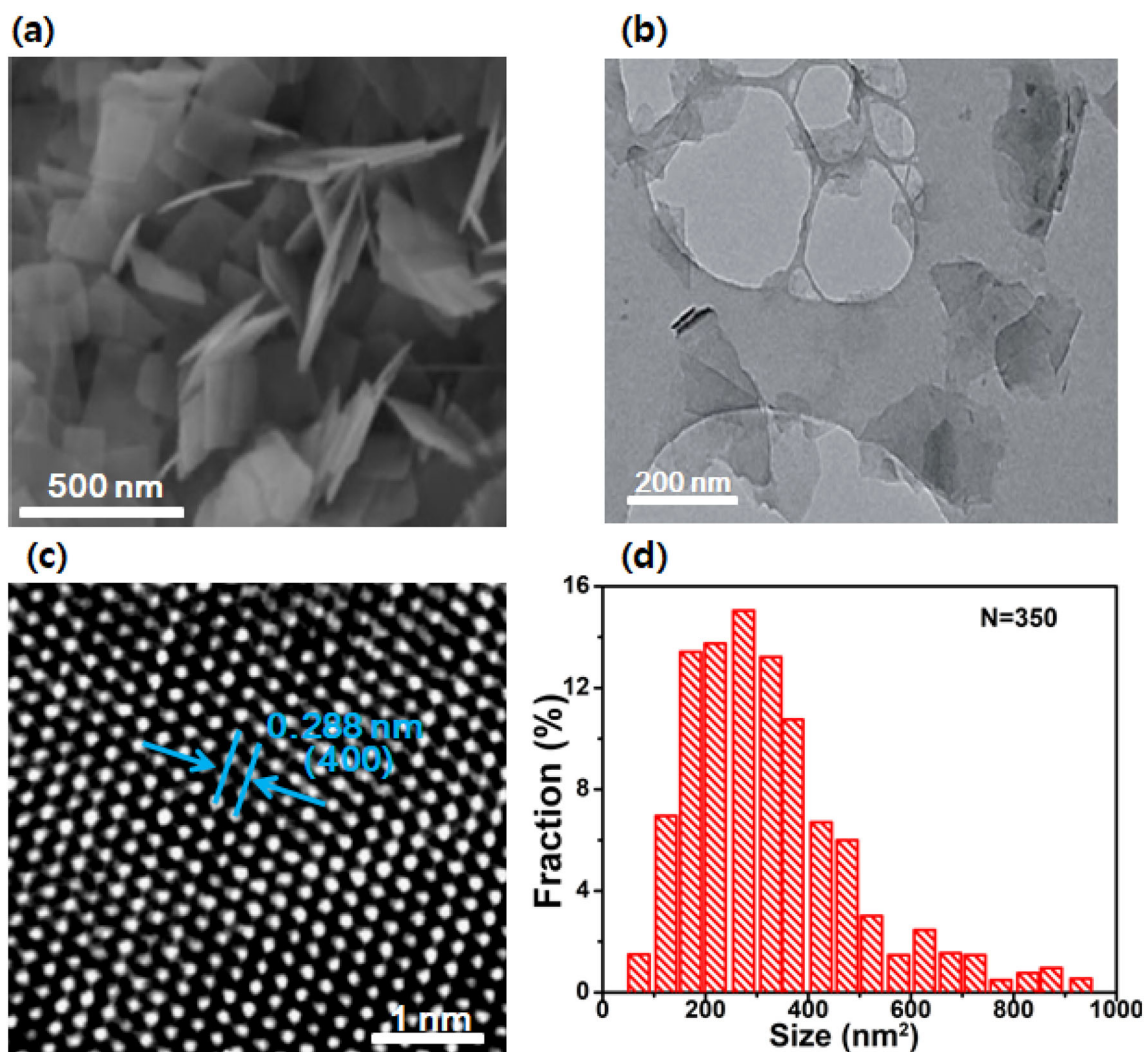
Fig. 2 **a** SEM image of exfoliated SnSe NSs, **b**, **c** TEM and HRTEM images of the as-obtained SnSe NSs, **d** Size distribution of the SnSe NSs was measured by TEM

crystalline orientation of the SnSe NSs. Raman spectrum was conducted on exfoliated SnSe NSs and bulk SnSe using a 532 nm-excitation-laser source with power of 0.5 mW to avoid damage of the samples. In Fig. 3d, the SnSe NSs exhibited four main peaks assigned to A_g^1, B_g^3, A_g^2, and A_g^3 [27, 28]. In comparison with bulk, while the B_g^3 and A_g^2 vibration modes of SnSe NSs show left shift, the right shift is clearly observed in the A_g^3 peak. The A_g^3 phonon mode corresponds to interlayer interaction along *a*-axis which weakened when the thickness of SnSe decreases. In contrast, the left shift of the B_g^3 and A_g^2 modes may originate from strengthening interlayer vibration of Sn and Se atoms in *b–c* plane which enhances within few layers. All the above evidences

demonstrate the high crystal quality of the as-synthesized SnSe NSs [29].

XPS was further employed to get inside the chemical composition of the exfoliated SnSe NSs. Figure 4a displays the high-resolution XPS spectra of Sn element which contains two peaks locating at 485.5 and 494.8 eV corresponding to Sn $3d_{5/2}$ and Sn $3d_{3/2}$, respectively. Furthermore, Se $3d_{5/2}$ and Se $3d_{3/2}$ of Se doublets (Fig. 4b) are observed at 54.2 and 53.3 eV, respectively. The atomic ratio between Sn and Se is determined by $N_{Sn}/N_{Se} = (I_{Sn}/S_{Sn})/(I_{Se}/S_{Se})$, where I is integral of peak intensity and S is relative sensitivity factors. The atomic ratio is calculated to be Sn:Se = 1:0.96.
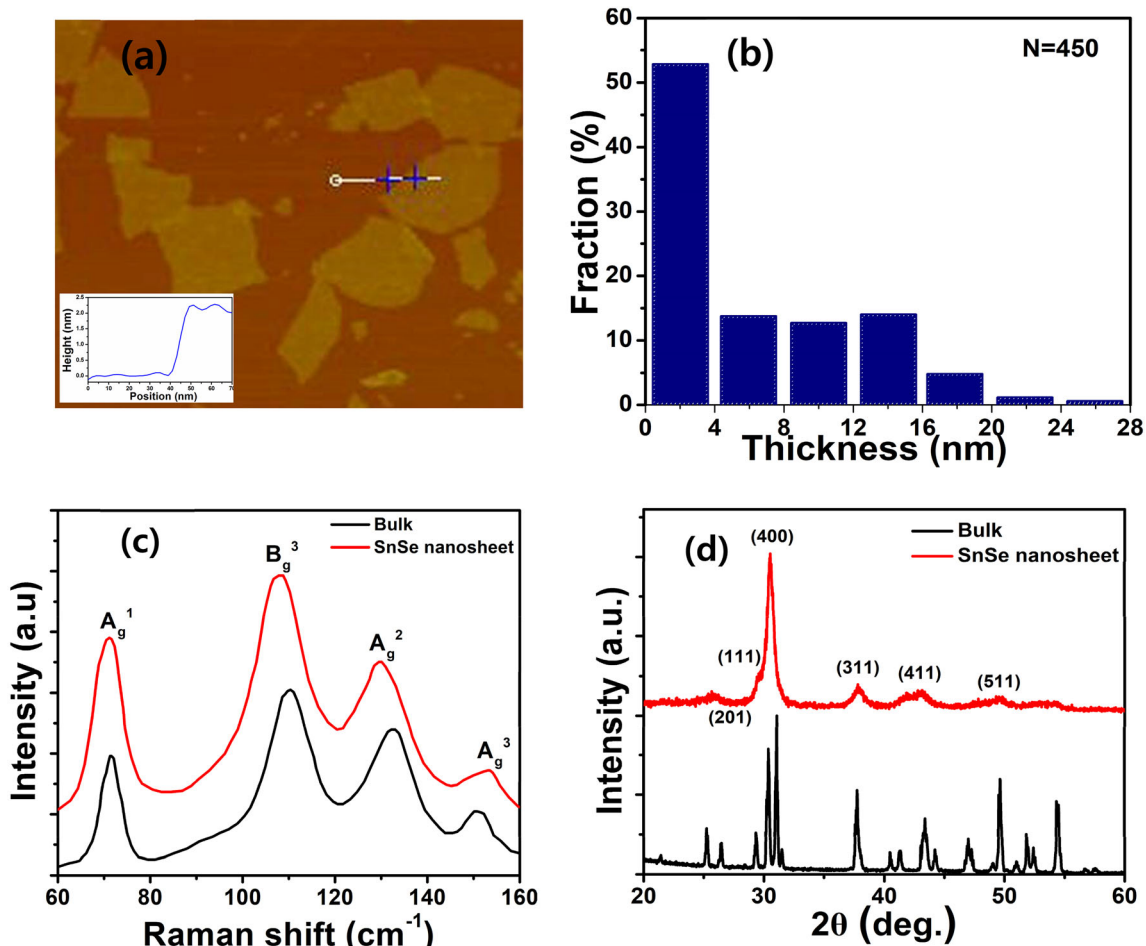
Fig. 3 **a** AFM image of a single SnSe NSs and inset the blue line displays the height profile across the NSs, **b** Thickness distribution of the SnSe NSs was measured by AFM, **c** Raman spectra of the SnSe NSs (red line) and SnSe bulk (black line), **d** The XRD characterization of SnSe NSs (red line) and the SnSe bulk (black line) (Color figure online)

To investigate the thermoelectric properties of the exfoliated SnSe NSs, SnSe-nanostructured-thin films were prepared with thicknesses between 350 and 650 nm. Figure 5 presents the thermoelectric properties of SnSe thin films in cross-plane direction as the function of temperature from 300 to 600 K. Before experiments, 450 nm sample was measured for 3 cycles on electrical conductivity and Seebeck coefficient to confirm the reliability of setup. In Fig. 5a, the electrical conductivity of all samples increases for higher temperature, it indicates the intrinsic property of semiconductor material. The sample with a thickness of 450 nm shows the highest σ value of 3.52 S/cm. Clearly, between 350 and 450 K, the electrical conductivity of this sample is relatively smaller than that of bulk SnSe. In contrast, the Seebeck coefficient of 450 nm sample exhibited the lowest value in that temperature range, as shown in Fig. 5b. The positive

Seebeck coefficients suggest p-type properties of the SnSe NSs. The PF of the 450 nm-sample reveals to the greatest value in temperature between 375 and 600 K. Accordingly to whole discussed data, it is concluded that 450 nm is the optimal thickness of the SnSe nanostructured thin film to obtain the highest thermoelectric efficiency at low-and-mid working temperature.

4 Conclusions

We have successfully synthesized SnSe NSs by using sonication-assisted exfoliation method with TBAB as intercalation molecules. During the sonication process, the TBA+ cations are inserted in interlayer of bulk SnSe and expanded lattice distance along a-axis causing exfoliation of bulk material into SnSe NSs
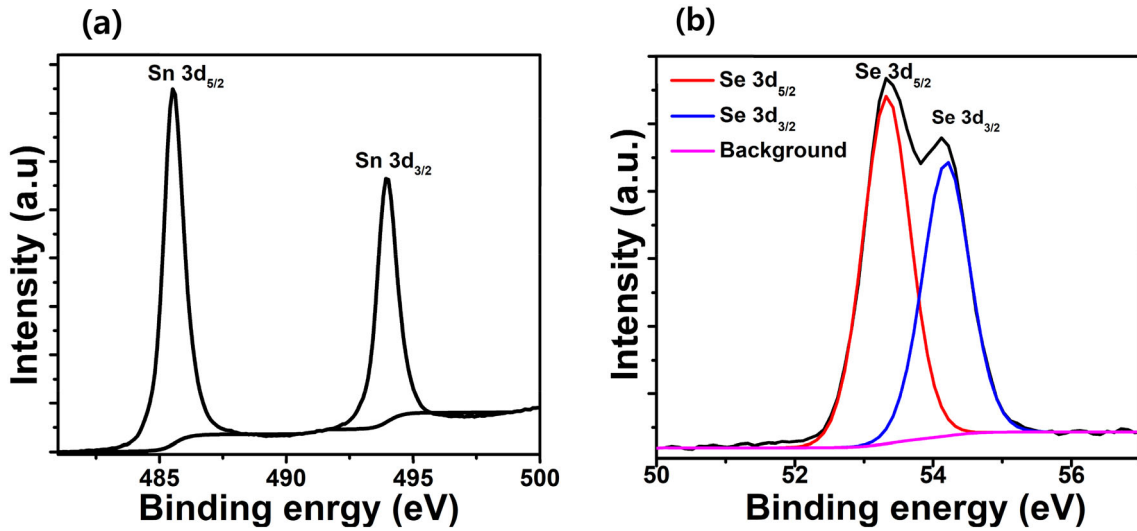
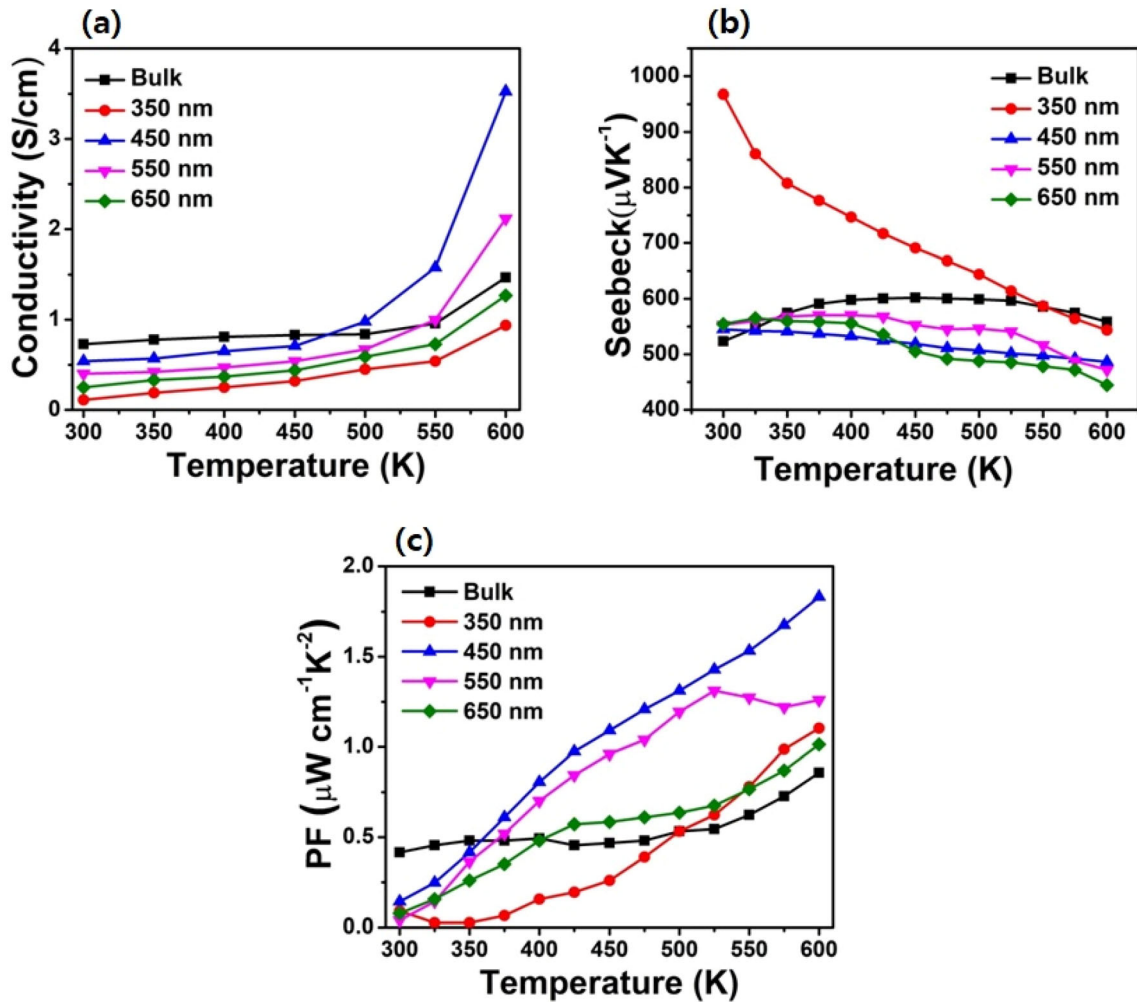Fig. 4 The XPS spectra of Sn (a) and Se (b) element of the SnSe NSs

Fig. 5 a, b Electrical conductivity and Seebeck coefficient of SnSe thin film at different thickness (350–650 nm) and bulk SnSe, c PF of various thickness samples

form. The obtained exfoliated SnSe NSs possess uniform lateral size of 280 nm^2 and thickness of few layers. The thickness of 450 nm thin film is optimized value for PF between 375 and 600 K. The results imply that the as-synthesized 2D SnSe possibly opens a new approach for fabricating SnSe-based thermoelectric devices.

Author contributions

TVD: Conceptualization, methodology, investigation, wrote, and edited of the manuscript. NXC wrote and edited of the manuscript. HNP, HTN, DDN, and LTL revised the manuscript and approved the final version of the manuscript. NVP designed the work, and revised the manuscript.

Funding

Data availability

All data available.

Declarations

Conflict of interest All authors declare that they have no conflict of interest.

References

1. I. Johnson, W.T. Choate, A. Davidson, in *Waste Heat Recovery, Technology and Opportunities in U.S. Industry* (BCS, Inc., Laurel, 2008), p. 112
2. A. Thekdi, S.U. Nimbalkar, in *Industrial Waste Heat Recovery, Potential Applications, Available Technologies and Crosscutting R&D Opportunities* (Oak Ridge National Lab. (ORNL), Oak Ridge, 2015), p. 82
3. S. Chu, Y. Cui, N. Liu, The path towards sustainable energy. Nat. Mater. **16**, 16–22 (2017)
4. J.S. Kang, M. Li, H. Wu, H. Nguyen, Y. Hu, Experimental observation of high thermal conductivity in boron arsenide. Science **361**, 575–578 (2018)
5. L.E. Bell, Cooling, heating, generating power, and recovering waste heat with thermoelectric systems. Science **321**, 1457–1461 (2008)
6. R. Venkatasubramanian, E. Siivola, T. Colpitts, B. O'Quinn, Thin-film thermoelectric devices with high room-temperature figures of merit. Nature **413**, 597–602 (2001)
7. L. Yang, Z.-G. Chen, M.S. Dargusch, J. Zou, High performance thermoelectric materials: progress and their applications. Adv. Energy Mater. **8**, 1701797 (2018)
8. T. Zhu, Y. Liu, C. Fu, J.P. Heremans, J.G. Snyder, X. Zhao, Compromise and synergy in high-efficiency thermoelectric materials. Adv. Mater. **29**, 1605884 (2017)
9. G. Homm, P.J. Klar, Thermoelectric materials—compromising between high efficiency and materials abundance, physica status solidi (RRL). Rapid Res. Lett. **5**, 324–331 (2011)
10. S.I. Kim, K.H. Lee, H.A. Mun, H.S. Kim, S.W. Hwang, J.W. Roh et al., Dense dislocation arrays embedded in grain boundaries for high-performance bulk thermoelectrics. Science **348**, 109–114 (2015)
11. C.B. Vining, An inconvenient truth about thermoelectrics. Nat. Mater. **8**, 83–85 (2009)
12. J.P. Heremans, B. Wiendlocha, A.M. Chamoire, Resonant levels in bulk thermoelectric semiconductors. Energy Environ. Sci. **5**, 5510–5530 (2012)
13. S. Hong, J. Park, S.G. Jeon, K. Kim, S.H. Park, H.S. Shin et al., Monolithic Bi$_{1.5}$Sb$_{0.5}$Te$_3$ ternary alloys with a periodic 3D nanostructure for enhancing thermoelectric performance. J. Mater. Chem. C **5**, 8974–8980 (2017)
14. A.F. Joffe, L.S. Stil'bans, Physical problems of thermoelectricity. Rep. Prog. Phys. **22**, 167–203 (1959)
15. L.D. Zhao, S.H. Lo, Y. Zhang, H. Sun, G. Tan, C. Uher et al., Ultralow thermal conductivity and high thermoelectric figure of merit in SnSe crystals. Nature **508**, 373–377 (2014)
16. C. Chang, M. Wu, D. He, Y. Pei, C.F. Wu, X. Wu et al., 3D charge and 2D phonon transports leading to high out-of-plane ZT in n-type SnSe crystals. Science **360**, 778–783 (2018)
17. L.-D. Zhao, C. Chang, G. Tan, M.G. Kanatzidis, SnSe: a remarkable new thermoelectric material. Energy Environ. Sci. **9**, 3044–3060 (2016)
18. W. Shi, M. Gao, J. Wei, J. Gao, C. Fan, E. Ashalley et al., Tin selenide (SnSe): growth, properties, and applications. Adv. Sci. **5**, 1700602 (2018)
19. Y. Xiao, C. Chang, Y. Pei, D. Wu, K. Peng, X. Zhou et al., Origin of low thermal conductivity in SnSe. Phys. Rev. B **94**, 125203 (2016)
20. S. Wang, S. Hui, K. Peng, T.P. Bailey, W. Liu, Y. Yan et al., Low temperature thermoelectric properties of p-type doped single-crystalline SnSe. Appl. Phys. Lett. **112**, 142102 (2018)

21. L.-D. Zhao, G. Tan, S. Hao, J. He, Y. Pei, H. Chi et al., Ultrahigh power factor and thermoelectric performance in hole-doped single-crystal SnSe. Science **351**, 141–144 (2016)

22. M. Kumar, S. Rani, Y. Singh, K.S. Gour, V.N. Singh, Tin-selenide as a futuristic material: properties and applications. RSC Adv. **11**, 6477–6503 (2021)

23. S. Liu, N. Sun, M. Liu, S. Sucharitakul, X.P.A. Gao, Nanostructured SnSe: synthesis, doping, and thermoelectric properties. J. Appl. Phys. **123**, 115109 (2018)

24. M. Gharsallah, F. Serrano-Sánchez, N.M. Nemes, F.J. Mompeán, J.L. Martínez, M.T. Fernández-Díaz et al., Giant seebeck effect in Ge-doped SnSe. Sci. Rep. **6**, 26774 (2016)

25. H. Ju, J. Kim, Chemically exfoliated SnSe nanosheets and their SnSe/Poly(3,4-ethylenedioxythiophene):Poly(styrene-sulfonate) composite films for polymer based thermoelectric applications. ACS Nano **10**, 5730–5739 (2016)

26. L. Li, Z. Chen, Y. Hu, X. Wang, T. Zhang, W. Chen et al., Single-layer single-crystalline SnSe nanosheets. J. Am. Chem. Soc. **135**, 1213–1216 (2013)

27. X. Gong, H. Wu, D. Yang, B. Zhang, K. Peng, H. Zou et al., Temperature dependence of Raman scattering in single crystal SnSe. Vib. Spectrosc. **107**, 103034 (2020)

28. B. Chakraborty, H.S.S.R. Matte, A.K. Sood, C.N.R. Rao, Layer-dependent resonant Raman scattering of a few layer MoS_2. J. Raman Spectrosc. **44**, 92 (2013)

29. D. Lu, C. Yue, S. Luo, Z. Li, W. Xue, X. Qi et al., Phase controllable synthesis of SnSe and $SnSe_2$ films with tunable photoresponse properties. Appl. Surf. Sci. **541**, 148615 (2021)